

Phasemeter based on second harmonic signal filter for space-based gravitational wave detection

Zheng Fan(范正), Zhu Li(李祝), Xiangqing Huang(黄祥青), Yurong Liang(梁浴榕), Yu Song(宋煜), Maomao Fan(范毛毛), Huizong Duan(段会宗), Siyuan Peng(彭思远), Shanqing Yang(杨山清), and Liangcheng Tu(涂良成)

Citation: Chin. Phys. B, 2026, 35 (**1**): 010601. DOI: 10.1088/1674-1056/ae1efe
http://cpb.iphy.ac.cn; http://iopscience.iop.org/cpb

What follows is a list of articles you may be interested in

Finite time hybrid synchronization of heterogeneous duplex complex networks via time-varying intermittent control

Cheng-Jun Xie(解成俊) and Xiang-Qing Lu(卢向清)
Chin. Phys. B, 2025, 34 (**4**): 040601. DOI: 10.1088/1674-1056/adacc6

A real-time performance improvement method for composite time scale

Fangmin Wang(王芳敏), Wenlin Li(李汶林), Hongfei Dai(戴鸿飞), Chunyi Li(李春怡), Jianhua Zhou(周建华), Shenhui Xue(薛申辉), and Bo Wang(王波)
Chin. Phys. B, 2024, 33 (**9**): 090601. DOI: 10.1088/1674-1056/ad6131

Physics package based on intracavity laser cooling ^{87}Rb atoms for space cold atom microwave clock

Siminda Deng(邓思敏达), Wei Ren(任伟), Jingfeng Xiang(项静峰), Jianbo Zhao(赵剑波), Lin Li(李琳), Di Zhang(张迪), Jinyin Wan(万金银), Yanling Meng(孟艳玲), Xiaojun Jiang(蒋小军), Tang Li(李唐), Liang Liu(刘亮), and Desheng Lü(吕德胜)
Chin. Phys. B, 2024, 33 (**7**): 070602. DOI: 10.1088/1674-1056/ad4bc1

Proposal for a realtime Einstein-synchronization-defined satellite virtual clock

Chenhao Yan(严晨皓), Xueyi Tang(汤雪逸), Shiguang Wang(王时光), Lijiaoyue Meng(孟李皎悦), Haiyuan Sun(孙海媛), Yibin He(何奕彬), and Lijun Wang(王力军)
Chin. Phys. B, 2024, 33 (**7**): 070601. DOI: 10.1088/1674-1056/ad3dc9

Michelson laser interferometer-based vibration noise contribution measurement method for cold atom interferometry gravimeter

Ning Zhang(张宁), Qingqing Hu(胡青青), Qian Wang(王倩), Qingchen Ji(姬清晨), Weijing Zhao(赵伟靖), Rong Wei(魏荣), Yuzhu Wang(王育竹)
Chin. Phys. B, 2020, 29 (**7**): 070601. DOI: 10.1088/1674-1056/ab8885

INSTRUMENTATION AND MEASUREMENT

Phasemeter based on second harmonic signal filter for space-based gravitational wave detection

Zheng Fan(范正)[1], Zhu Li(李祝)[1,†], Xiangqing Huang(黄祥青)[1], Yurong Liang(梁浴榕)[2], Yu Song(宋煜)[1], Maomao Fan(范毛毛)[1], Huizong Duan(段会宗)[1], Siyuan Peng(彭思远)[1], Shanqing Yang(杨山清)[1], and Liangcheng Tu(涂良成)[1]

[1] *MOE Key Laboratory of Tianqin Mission, Frontiers Science Center for Tianqin, CNSA Research Center for Gravitational Waves, Tianqin Research Center for Gravitational Physics, School of Physics and Astronomy, Sun Yat-sen University (Zhuhai Campus), Zhuhai* 519082, *China*

[2] *Center for Gravitational Experiment, MOE Key Laboratory of Fundamental Physical Quantities Measurements, The School of Physics, Huazhong University of Science and Technology, Wuhan* 430074, *China*

(Received 6 August 2025; revised manuscript received 30 September 2025; accepted manuscript online 13 November 2025)

The space gravitational wave detection aims to detect gravitational waves in the mHz band in order to study supermassive black hole mergers, galaxy evolution and the structure of the early universe. One of its core payloads is a transponder-type interstellar laser interferometer, designed to measure relative displacement changes at the pico-meter level. Among its components, phasemeter is tasked with extracting the phase and frequency of the interference signal. Currently, phase-locked loop (PLL) phasemeters are commonly employed. However, the second harmonic signal generated by the mixer can restrict both the dynamic range and phase measurement accuracy of the phasemeter. This paper analyzes the interstellar laser interferometer and the impact of the second harmonic signal on the phasemeter's performance. To address these challenges, a phasemeter incorporating a second harmonic signal filter is proposed. This new design mitigates second harmonic disturbances within the phasemeter's bandwidth by dynamically adjusting the filter's cutoff frequency to track the input signal frequency, thereby suppressing the second harmonic signal in real time. Theoretical and simulation analyses demonstrate that the proposed phasemeter with a second harmonic filter significantly enhances the dynamic range. Finally, experimental results verify that the phasemeter can achieve the tracking of sudden frequency changes up to 4.8 MHz.

Keywords: laser interferometer, phasemeter, second harmonic signal, dynamic range

PACS: 06.30.Ft, 04.80.Nn, 07.60.Ly

DOI: 10.1088/1674-1056/ae1efe **CSTR:** 32038.14.CPB.ae1efe

1. Introduction

Space-based gravitational wave detection (SGWD) is expected to be realized in the 0.1 mHz to 1 Hz frequency band,[1,2] targeting a range of astrophysical events,[3–7] including the inspiral of compact galactic binaries, the coalescence of stellar-mass binary black holes, the merger of massive binary black holes, extreme mass ratio inspirals, and phase transition processes in the early universe. Currently, the major international SGWD missions include LISA,[8] TianQin,[9] DECIGO,[10] and Taiji.[11] The TianQin project, proposed by Chinese scientists,[9] aims to launch three identical satellites by 2035 to form a space-based gravitational wave observatory. Detection is achieved using an interstellar laser interferometer with an arm length of approximately 170000 km. Variations in satellite separation are measured through the phase signal of the heterodyne laser interferometer's beat-frequency signal. To meet the scientific objectives, the displacement sensitivity of the interstellar laser interferometer is required to reach 1 pm/Hz$^{1/2}$.[12] Additionally, the phasemeter noise must be below 5 μrad/Hz$^{1/2}$,[13] considering factors such as laser frequency stability, relative intensity noise, and arm length fluctuations. Beyond gravitational wave detection, phasemeters in SGWD can also be utilized for laser pointing, data communications, global navigation satellite system applications, and absolute interstellar distance measurements.

Phasemeters used in SGWD require exceptionally high phase measurement accuracy.[13] Researchers have conducted various studies on phasemeter phase measurement precision, including works from AEI,[14–16] HUST,[17–19] Chinese Academy of Sciences,[20] and SYSU.[21] Currently, phasemeters have achieved phase measurement accuracies of 0.7 μrad/Hz$^{1/2}$ at 0.1 Hz and 5 μrad/Hz$^{1/2}$ at 1 mHz.[18] Although phasemeters have achieved exceptionally high precision in phase measurements, their adaptability for application in space science experiments remains to be investigated. In the SGWD, the relative velocity variations between satellites induce a Doppler shift in the propagating laser signals.[22,23] The Doppler frequency due to interstellar relative motion is about 10 MHz.[22,23] To ensure that the phasemeter can operate under varying degrees of interstellar relative motion, phaseme-

†Corresponding author. E-mail: lizhu@mail.sysu.edu.cn

© 2026 Chinese Physical Society and IOP Publishing Ltd. All rights, including for text and data mining, AI training, and similar technologies, are reserved.

ters used for space gravitational wave detection need to operate within a large signal frequency range below 25 MHz. Consequently, in addition to high-precision phase measurement capabilities, phasemeters must also feature a large dynamic range and strong resistance to sideband signal interference. The commonly used sine multiplication demodulation method generates a second harmonic signal below the 50 MHz frequency range, which overlaps with the operational frequency measurement range (below 25 MHz). To mitigate the adverse effects of second harmonic interference on phasemeter readout accuracy, an effective filtering mechanism is required.

In phasemeters utilizing sine multiplication demodulation, a low-pass filter with a fixed cutoff frequency is typically employed to suppress the second harmonic signal.[24] To minimize loop noise, the cutoff frequency of the low-pass filter must be kept as low as possible. However, during abrupt frequency changes, the low-pass filter may inadvertently suppress phase error signals, leading to inaccurate phase and frequency readouts.[25] Additionally, the phase-frequency response of the low-pass filter introduces phase delays within the loop, which in turn reduces the dynamic range of the phasemeter's frequency measurements. Given these challenges, it is essential to assess the impact of second harmonic interference on phasemeter performance and explore alternative filtering methods to effectively mitigate this issue.

In this paper, a phasemeter incorporating a second harmonic filter is proposed. To mitigate second harmonic interference within the phasemeter's bandwidth, the cutoff frequency of the newly designed filter dynamically adapts to the input signal frequency, enabling real-time suppression of the second harmonic component. The paper is structured as follows. Section 2 examines the application background of the phasemeter and the mechanism by which second harmonic interference affects its performance. Section 3 analyzes the characteristics and noise performance of the phasemeter equipped with a second harmonic filter. In Section 4, a phasemeter model incorporating the second harmonic filter is developed, and digital fixed-point simulations are conducted to validate its functionality. Compared to conventional phasemeters, the proposed design achieves real-time second harmonic suppression without attenuating the fundamental frequency signal, ensuring effective frequency tracking and phase locking.

2. Interstellar laser interferometer and phasemeter principle

In the SGWD, the interstellar laser interferometer operates based on the transponder-type laser interferometry principle, necessitated by the 170000 km separation between satellites and the inevitable laser beam divergence.[12] As illustrated in Fig. 1, the master satellite emits a laser beam, which propagates across the large intersatellite distance and is received by the telescope of the slave satellite. The received beam is then combined with the local laser in the slave satellite for heterodyne interferometry. The resulting optical interference signals are detected by a quadrant photodetector (QPD) and converted into electrical signals. A phase measurement system extracts the phase and frequency information

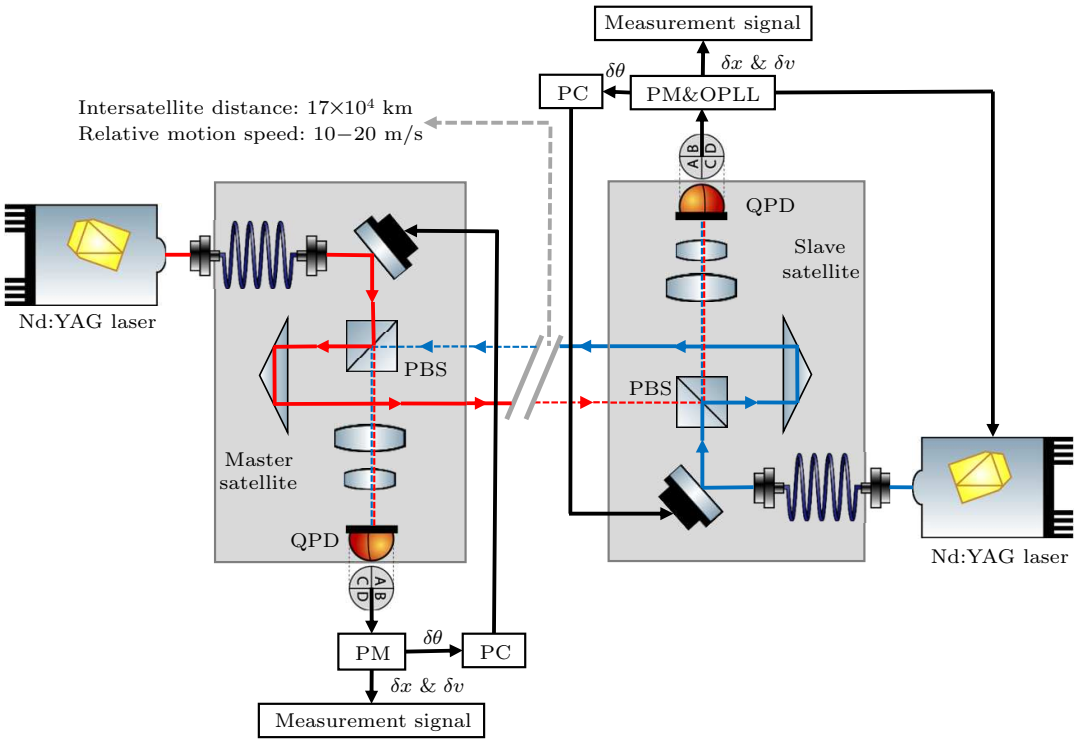


Fig. 1. Principle of a transponder-type interstellar laser interferometer.

from these signals. The phase signal is subsequently phase-locked to the slave satellite's laser using an optical phase-locked loop (OPLL). The slave satellite then retransmits the laser back to the master satellite, where it is again received by the master satellite's telescope and combined with its local laser for heterodyne interferometry. The optical interference signals are processed similarly — converted by the QPD into electrical signals, with the phase and frequency readout completed by the phase measurement system. Beyond phase measurement, phasemeters in transponder-based interstellar laser interferometers also play a crucial role in intersatellite laser beam pointing and alignment.[26–30]

To accommodate the relative motion between satellites, the phase-locked loop (PLL) principle is employed to achieve a wide frequency measurement range in the phasemeter. As illustrated in Fig. 2,[24] the QPD receives the optical interference signal and converts it into a weak electrical current. This signal is then processed through an interface circuit and an anti-aliasing filter before being digitized by an analog-to-digital converter (ADC) and fed into the FPGA-based digital phasemeter. In a PLL-based phasemeter, the phase detector consists of a mixer followed by a low-pass filter (LPF). The phase detector (PD) processes the interference signal and the numerically controlled oscillator (NCO) signal to compute the phase error. This phase error signal is then fed into a proportional-integral (PI) controller, which generates a control signal that drives the NCO. The NCO produces an oscillating signal that remains synchronized in both frequency and phase with the interference signal.[31]

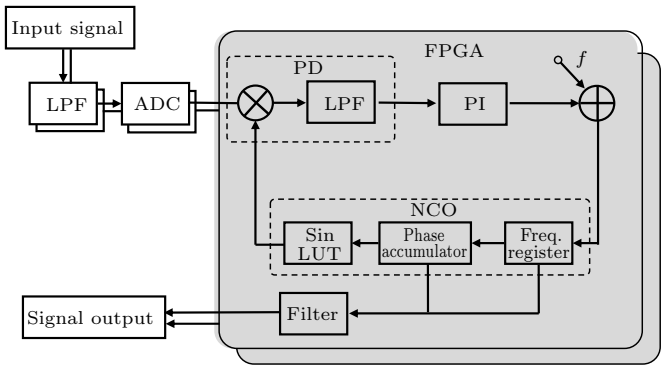


Fig. 2. Principle of all-digital phase measurement system.

The second harmonic signal is generated within the mixer when the interference signal and the NCO signal are multiplied, which can be expressed as

$$\begin{aligned} u_{\rm mux}(t) &= u_i(t)\cdot u_{\rm NCO}(t) \\ &= A\sin[\omega_0(t)+\theta_i(t)]\cdot\cos[\omega_0(t)+\theta_{\rm NCO}(t)] \\ &= A/2\sin[\theta_{\rm e}(t)] \\ &\quad + A/2\sin[2\omega_0(t)+\theta_i(t)+\theta_{\rm NCO}(t)], \end{aligned} \tag{1}$$

where the second harmonic signal part of Eq. (1) is

$$u_{{\rm mux},2f}(t) = A/2\sin[2\omega_0(t)+\theta_i(t)+\theta_{\rm NCO}(t)]. \tag{2}$$

The second harmonic signal is transmitted through the phase-locked loop for a time $\tau_{\rm g}$ and produces an effective phase modulation. Assuming that $\tau_{\rm g}$ is a constant and the reciprocal of the effective frequency $\omega_{\rm eff}$ is numerically smaller than $\tau_{\rm g}$, the effective parasitic phase error can be approximated as[16]

$$\theta_{{\rm e},2f}(t) \approx \frac{H_{\rm open}(2\omega_{\rm eff})}{4}\sin[\omega_{\rm eff}(t)\cdot\tau_{\rm g}], \tag{3}$$

where $H_{\rm open}(2\omega_{\rm eff})$ is the attenuation parameter of the second harmonic frequency through the phase-locked loop open-loop transfer function, and the open-loop gain of the error signal in the low-frequency band is ~ 1. $H_{\rm open}$ represents the product of the phase detector transfer function, the PI controller transfer function, and the NCO transfer function within the phase-locked loop. The proportional and integral coefficients within the PI controller primarily influence $H_{\rm open}$.

From the above analysis, it can be seen that this parasitic phase coupling noise is highly nonlinear. And its magnitude is highly dependent on the loop's suppression of the second harmonic frequency, the signal transmission delay in the phase-locked loop, and the dynamics of the input signal $\omega_{\rm eff}$. This coupling effect is most pronounced for sinusoidal signals. Assuming sinusoidal signal input operating conditions, the noise spectral density of the parasitic phase error can be expressed as[16]

$$\tilde{\theta}_{{\rm e},2f}(f) \approx \frac{H_{\rm open}(2\omega_{\rm eff})}{4}\sin[\tilde{\omega}_{\rm eff}(f)\cdot\tau_{\rm g}]. \tag{4}$$

Additionally, the second harmonic signal introduces an extra root mean square value to the phase signal. While it does not directly contribute to phase error within the spatial gravitational wave detection range, it increases the likelihood of the PD deviating from its linear operating range within the bandwidth of the LPF. The maximum additional error can be expressed as[16]

$$\theta_{{\rm e},2f\,\max} = H_{\rm open}(2\omega_{\rm eff}). \tag{5}$$

Based on the above analysis, the influence mechanism of the second harmonic signal on the phase error signal can be determined. In SGWD, the interference signal bandwidth, ranging below 25 MHz due to the relative motion between satellites, necessitates an LPF cutoff frequency greater than 20 MHz to ensure accurate phase readout and locking over a wide signal bandwidth. However, second harmonic signals below 20 MHz will fall within the LPF passband. Moreover, an excessively high LPF cutoff frequency introduces additional noise into the loop, further affecting measurement accuracy. To simultaneously achieve effective second harmonic suppression and maintain a wide dynamic frequency range for phase readout, a dedicated filter designed specifically for second harmonic signal suppression is required.

3. Characteristics of second harmonic signal filters

3.1. Principle of second harmonic signal filters

To effectively suppress the second harmonic signal while ensuring PD performance over a wide interference signal frequency range below 25 MHz, a PD based on a second harmonic signal filter is proposed. Figure 3 illustrates the schematic of the phasemeter incorporating the second harmonic signal filter. The interstellar laser interference signal is first processed by the QPD and the interface circuit, then sampled as digital signals by the ADC and input into the PD. The PD consists of a mixer coupled with the second harmonic signal filter, and the processed signal passes through the PD to generate a phase error signal. This phase error signal is then input into a PI controller, which produces control signals that are sent to the NCO and a second NCO operating at double the frequency. The NCO generates an oscillating signal synchronized with the frequency and phase of the interference signal, which is mixed with the interference signal in the PD. Meanwhile, the two-fold frequency NCO generates a signal matching the second harmonic frequency, which is input into each of the two mixers in the second harmonic signal filter. Ultimately, the second harmonic is subtracted via the subtractor.

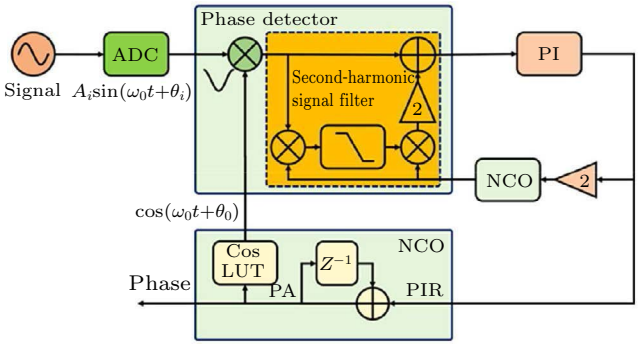


Fig. 3. Principle of phasemeter based on second harmonic signal filters.

In the PD based on the second harmonic signal filter, the mixer multiplies the interfering signal $u_i(t)$ with the NCO signal $u_{\rm NCO}(t)$:

$$\begin{aligned} u_{\rm mux}(t) &= u_i(t)\cdot u_{\rm NCO}(t) \\ &= A\sin[\omega_0(t)+\theta_i(t)]\cdot\cos[\omega_0(t)+\theta_{\rm NCO}(t)] \\ &= A/2\sin[\theta_{\rm e}(t)]+A\,2\sin[2\omega_0(t)+\theta_{\rm e}(t)], \end{aligned} \tag{6}$$

where the mixer signal $u_{\rm mux}(t)$ includes the phase error signal and the second harmonic signal. The mixer signal $u_{\rm mux}(t)$ is input to the second harmonic signal filter. The mixer signal $u_{\rm mux}(t)$ is obtained by multiplying it with the second harmonic NCO signal:

$$\begin{aligned} u_{2f{\rm mux}}(t) &= u_{\rm mux}(t)\cdot u_{2f{\rm NCO}}(t) \\ &= \sin[2\omega_0(t)]\cdot A/2\{\sin[\theta_{\rm e}(t)]+\sin[2\omega_0(t)+\theta_{\rm e}(t)]\} \\ &= A/4\cdot\{\cos[\theta_{\rm e}(t)]+\cos[2\omega_0(t)-\theta_{\rm e}(t)] \\ &\quad -\cos[2\omega_0(t)+\theta_{\rm e}(t)]-\cos[4\omega_0(t)+\theta_{\rm e}(t)]\}. \end{aligned} \tag{7}$$

It can be seen that the two-fold frequency mixing signal $u_{2f{\rm mux}}(t)$ consists of the phase error signal, the second harmonic signal, and the fourth harmonic signal. When the loop achieves lock, the phase error is close to zero and the second harmonic signal is negligible. When the two-fold frequency mixing signal $u_{2f{\rm mux}}(t)$ passes through the LPF, the fourth harmonic signal can be filtered out:

$$u_{2f{\rm LPF}}(t)\approx A/4\cdot\cos[\theta_{\rm e}(t)]. \tag{8}$$

The signal $u_{2f{\rm LPF}}(t)$ after the low-pass filter is multiplied by the two-fold frequency NCO signal:

$$\begin{aligned} u_{2f2{\rm ndmux}}(t) &= u_{2f{\rm NCO}}(t)\cdot u_{2f{\rm LPF}}(t) \\ &= \sin[2\omega_0(t)]\cdot A/4\cos[\theta_{\rm e}(t)] \\ &= A/8\cdot\{\sin[2\omega_0(t)+\theta_{\rm e}(t)] \\ &\quad +\sin[2\omega_0(t)-\theta_{\rm e}(t)]\} \\ &\approx A/4\cdot\sin[2\omega_0(t)]. \end{aligned} \tag{9}$$

Similarly, when the loop is locked, the two-fold frequency second mixed signal $u_{2f2{\rm ndmux}}(t)$ contains only the second harmonic signal. In order to achieve the two-fold frequency signal subtraction, it is necessary to keep the amplitude level of the two-fold frequency second mixing signal $u_{2f2{\rm ndmux}}(t)$ the same as that of the second harmonic signal in the mixer signal $u_{\rm mux}(t)$. The two-fold frequency second mixing signal $u_{2f2{\rm ndmux}}(t)$ needs to be amplified in amplitude and subtracted from the mixer signal $u_{\rm mux}(t)$:

$$\begin{aligned} u_{\rm PD}(t) &= u_{\rm mux}(t)-2\cdot u_{2f2{\rm ndmux}}(t) \\ &= A/2\sin[\theta_{\rm e}(t)]+A/2\sin[2\omega_0(t)+\theta_{\rm e}(t)] \\ &\quad -A/2\cdot\sin[2\omega_0(t)] \\ &\approx A/2\sin[\theta_{\rm e}(t)]. \end{aligned} \tag{10}$$

When the loop achieves phase lock, the phase error is close to 0, which enables the subtraction of the second harmonic signal generated by the mixer to obtain the phase error signal.

Compared to the normal PD phasemeter, the new PD phasemeter can achieve fast tracking under large frequency changes. The filtering of the second harmonic in the normal PD phasemeter relies on the LPF, and in order to achieve the effective filtering of the second harmonic, a lower low-pass filter cut-off frequency is required. In contrast, the second harmonic filtering in the new PD phasemeter is deducted by subtracting the mixer signal $u_{\rm mux}(t)$ from the two-fold frequency second mixing signal $u_{2f2{\rm ndmux}}(t)$. The effect of the subtraction of the second harmonic signal does not depend entirely on the LPF and does not require a cut-off frequency as low as the LPF in the normal PD phasemeter. From the above analysis,

it can be learned that the LPF in the normal PD phasemeter needs to have a low cut-off frequency. And the lower the cut-off frequency of the LPF, the greater the delay caused by this filter will be. The new PD phasemeter reduces the loop phase delay to achieve greater frequency tracking capability.

3.2. Noise analysis of new PD phasemeter

The new PD phasemeter is designed for space gravitational wave detection, which demands high-precision phase measurement. As such, a detailed analysis of its phase noise is essential. Crucially, compared to the normal PD phasemeter, the architectural improvements in the new design do not introduce additional phase noise sources. The sources of noise in the phasemeter based on the second harmonic signal filter are mainly the quantization noise and sampling time jitter noise in the ADC, and the down-sampling read noise at the phase signal output. The quantization noise is related to the sampling rate and effective bit width of the ADC and can be expressed as[25]

$$\sqrt{S^{V}_{\text{quan}}} = \frac{q}{\sqrt{6f_{\text{s}}}} \ [\text{V}/\text{Hz}^{1/2}], \tag{11}$$

where q denotes the minimum quantization step, $q = V_{\text{pp}}/2^{N}$, where N denotes the number of effective bits of the ADC. The quantization noise is treated as additive noise, again $V_{\text{s}} = 0.5V_{\text{pp}}$. Therefore, the expression for the conversion of quantization noise to phase noise can be expressed as[25]

$$\sqrt{S^{\Phi}_{\text{quan}}} = \frac{V_{\text{pp}}}{2^{N}\sqrt{6f_{\text{s}}}}\frac{1}{V_{\text{s}}} \ [\text{rad}/\text{Hz}^{1/2}]. \tag{12}$$

Sample time jitter noise is a deviation from the ideal sampling interval due to clock instability. Its contribution to the phase noise can be expressed as[21]

$$\Phi_{\text{jit}} = 2\pi f_{\text{h}}\tau \ [\text{rad}], \tag{13}$$

where f_{h} is the heterodyne frequency, and τ is the sampling time jitter noise.

The phase readout noise is the read noise after downsampling the output phase of the phasemeter through the CIC filter, and this part of the noise is mainly quantization noise, denoted as[25]

$$\begin{aligned}\sqrt{S^{\Phi}_{\text{read}}} &= \frac{q}{\sqrt{6f_{\text{s}}}} \\ &= \frac{2\pi}{2^{M}}\frac{1}{\sqrt{6f_{\text{s}}}} \ [\text{rad}/\text{Hz}^{1/2}].\end{aligned} \tag{14}$$

In addition to this, temperature drift also affects the phasemeter. Temperature as a slowly varying signal affects the phasemeter mainly in the low frequency band below 1 mHz and depends mainly on the temperature environment.[32] Limiting the effects of temperature drift can be achieved by additional temperature control. Since the new PD phasemeter is optimized and improved only on the PD, there is no difference in the noise source compared to the normal PD phasemeter. Table 1 presents the phasemeter noise calculation. The noise is analyzed using typical phasemeter parameters, and it is observed that the primary noise source is the sampling time jitter noise. This jitter noise can be mitigated through pilot-tone correction,[17,18] and previous studies[21] have demonstrated that such a method can reduce the noise level to 5 μrad/Hz$^{1/2}$.

Table 1. Phase noise calculation of second harmonic signal filter-based phasemeter.

Noise sources	Noise expression	Typical parameters	Noise level
Quantization noise	$\sqrt{S^{\Phi}_{\text{quan}}} = \frac{V_{\text{pp}}}{2^{N}\sqrt{6f_{\text{s}}}}\frac{1}{V_{\text{s}}}$	$f_{\text{s}} = 125$ MHz, $N = 16$ bit	2.8×10^{-10} rad/Hz$^{1/2}$
Sampling time jitter	$\Phi_{\text{jit}} = 2\pi f_{\text{h}}\tau$	$f_{\text{h}} = 10$ MHz, $\tau = 5\times10^{-13}$ s/Hz$^{1/2}$	3.1×10^{-5} rad/Hz$^{1/2}$
Phase readout noise	$\sqrt{S^{\Phi}_{\text{read}}} = \frac{2\pi}{2^{M}}\frac{1}{\sqrt{6f_{\text{s}}}}$	$f_{\text{s}} = 10$ Hz, $M = 24$ bit	4.8×10^{-8} rad/Hz$^{1/2}$

4. Digital fixed-point simulation and verification

4.1. Digital fixed-point simulation model

The new PD phasemeter is modeled and simulated using MATLAB and Simulink. Based on the principle of the phasemeter with the second harmonic signal filter, as shown in Fig. 3, the PD subsystem, PI controller subsystem, and NCO subsystem were modeled individually. Figure 4 presents the Simulink simulation model for the phasemeter incorporating the second harmonic signal filter. As depicted in Fig. 3, the PD subsystem integrates the mixer with the second harmonic signal filter, enabling the phase discriminator function based on the second harmonic signal filter. The inputs to the PD subsystem include the laser interferometric discrete signals, the NCO cosine signal, the sine and cosine signals from the two-fold frequency NCO, with the output being the phase error signal. The PI controller subsystem includes both proportional and integral control, allowing for the conversion of phase error signals into control signals. The NCO subsystem integrates both the NCO and the two-fold frequency NCO. The NCO consists of a phase increment register (PIR), a phase accumulator (PA), and a look-up table (LUT). The inputs to the NCO subsystem are the control signal and the initial frequency signal f, with the outputs being the phase, the NCO cosine signal, and the sine and cosine signals from the two-fold frequency NCO. Table 2 presents the parameters used in the Simulink simulation model.

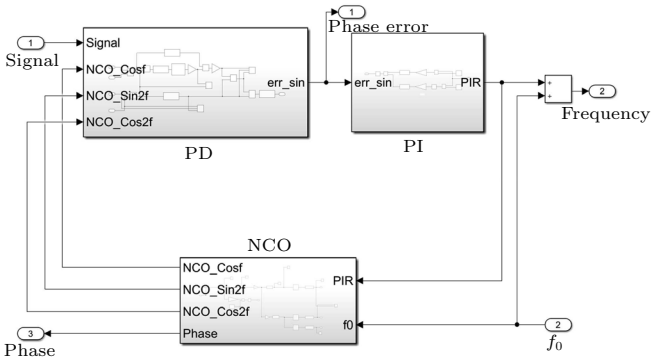


Fig. 4. Simulation model of phasemeter based on the second harmonic signal filter.

Table 2. Simulation parameters of second harmonic signal filter-based phasemeter.

Parameter	Value
Sampling rate	125 MSPS
Bit width of ADC	16 bits
Bit width of sin&cos LUT	12 bits
Heterodyne frequency	10.62 MHz
Amplitude of signal	0.5 V
Input range of ADC	2 Vpp
LPF cut-off frequency of normal PD	0.1 MHz
LPF cut-off frequency of new PD	10 Hz

4.2. Simulation verification of frequency change

To verify the anti-interference capability of the phasemeter based on the second harmonic signal filter, simulations of phase locking and readout performance were conducted under conditions of a sudden, large frequency change in the interfering signal. The interfering signal $u_i(t)$ was input into two phasemeters, each based on different types of PD. The initial conditions are set as follows: the initial frequency signal input f is 10 MHz and the heterodyne frequency is 10.62 MHz. By monitoring the frequency readout of the phasemeter, the frequency tracking capability was evaluated. Figure 5 illustrates the frequency response capabilities of the two phasemeters. In the normal PD phasemeter, the phase error signal is filtered out by the LPF when the signal frequency undergoes a significant change. As shown in Fig. 5, the normal PD phasemeter attempts to control the opposite frequency. In contrast, the new PD phasemeter employs a real-time subtraction method to remove the second harmonic signal from the mixer, allowing the phase error signal to be obtained. As a result, frequency tracking continues, and re-locking is successfully achieved within 7.5 ms. In order to analyze the frequency tracking performance of the new PD phasemeter in the frequency band below 25 MHz, a frequency change of 0.62 MHz is applied at the base frequencies of 5 MHz, 15 MHz, 20 MHz, and 24 MHz respectively. Figures 5(b)–5(e) show the frequency tracking performance of the new PD phasemeter at 5 MHz, 15 MHz, 20 MHz, and 24 MHz, respectively. It can be clearly seen that the new PD phasemeter can achieve fast tracking of frequency change in the frequency band below 25 MHz. Moreover, the frequency tracking times are all within 10 ms. The delay time is due to the fact that the new PD phasemeter is temporary unlocking after a sudden frequency change. Within a short period of time, the new PD phasemeter will quickly track the frequency change and achieve re-locking. In order to analyze the frequency tracking performance of the new PD phasemeter in the case of large frequency mutations, a frequency change of 4.8 MHz is applied to a frequency of 10.1 MHz to analyze the frequency readout of the new PD phasemeter. Figure 5(f) demonstrates the frequency tracking performance of the new PD phasemeter under a large frequency change of 4.8 MHz, where frequency re-tracking is achieved in a short period of time. After the sudden frequency change, the frequency readout of the new PD phasemeter gradually tracks from 10.1 MHz to 14.9 MHz, proving that the new PD phasemeter can cope with the sudden frequency change of 4.8 MHz.

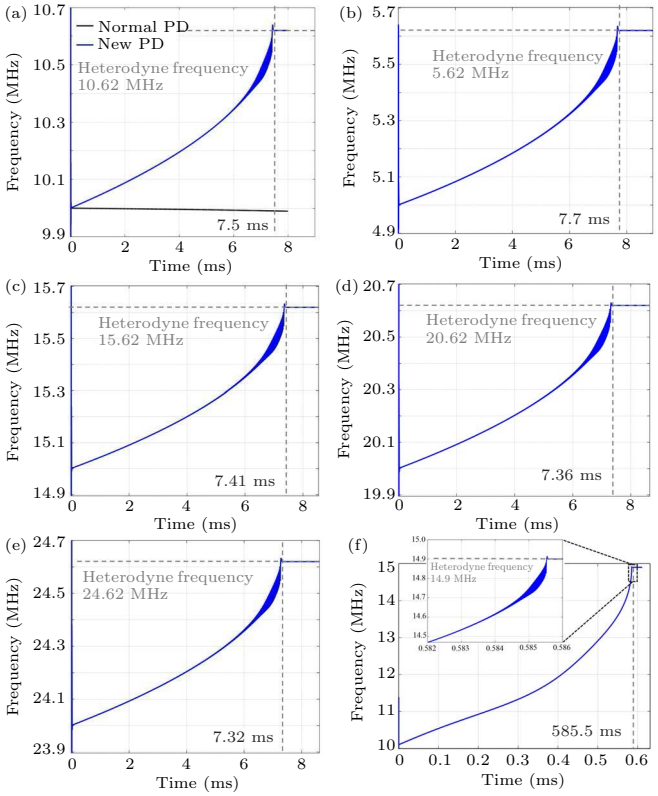


Fig. 5. Frequency tracking performance of the new PD phasemeter. (a) Comparison of the frequency tracking ability of two phasemeters when the signal frequency changes abruptly from 10 MHz to 10.62 MHz. (b)–(e) Frequency tracking performance of the new PD phasemeter at (b) 5 MHz, (c) 15 MHz, (d) 20 MHz, and (e) 24 MHz in response to the signal frequency abrupt changes. (f) Frequency tracking performance of the new PD phasemeter when the signal frequency changes abruptly from 10.1 MHz to 14.9 MHz.

For the normal PD phasemeter, the cut-off frequency of the low-pass filter used for second-harmonic filtering affects frequency tracking after sudden frequency changes. If its cut-off frequency is low, the phase error signal will be filtered out when a large frequency change occurs, affecting frequency tracking. However, the maximum frequency tracking performance of the new PD phasemeter is not limited by the LPF

and is directly related to the ADC sampling rate, which can satisfy the effects caused by large frequency changes. Since the second harmonic filtering of the new PD is achieved by subtracting mixer signal $u_{\mathrm{mux}}(t)$ from the two-fold frequency second mixing signal $u_{2f2\mathrm{ndmux}}(t)$, where the LPF does not directly cause the deduction of the error signal. The two-fold frequency second mixing signal $u_{2f2\mathrm{ndmux}}(t)$ likewise tracks the second harmonic signal in the mixer signal $u_{\mathrm{mux}}(t)$. In summary, the key advancement of the new PD phasemeter lies in its adaptive second-harmonic filter, which presents a fundamental improvement over the static low-pass filter (LPF) used in conventional designs. Unlike the fixed-cutoff LPF in a normal PD phasemeter, the harmonic cancelation in our new design dynamically adjusts with the input signal. This effectively creates an equivalent LPF with a cutoff frequency that tracks the signal in real-time. This innovation ensures robust suppression of the second-harmonic interference while preventing the accidental attenuation of the essential phase error signal during frequency transients. Crucially, this enhanced stability is achieved without altering the fundamental noise sources or compromising the intrinsic phase readout performance. Therefore, the proposed phasemeter architecture significantly improves the operational robustness and reliability required for the demanding environment of space-based gravitational wave detection.

Figure 6 illustrates the phase error of the new PD phasemeter. Figure 6(a) shows the phase error following a sudden change in frequency, while Fig. 6(b) displays the phase error after phase lock has been achieved. When a sudden change in frequency occurs, the phase error of the new PD phasemeter becomes larger, causing the new PD phasemeter to temporarily lose lock. The NCO in the new PD phasemeter will gradually track the interference signal until re-lock is achieved. For the phasemeter utilizing the new subtraction method, the phase error eventually approaches 0 rad after prolonged loop control, confirming that phase lock is successfully established. In Fig. 6(a), the phase error is initially large, approximately 5 rad, before phase lock is achieved at 7.5 ms. Once the phase error approaches 0 rad after 7.5 ms, phase lock is successfully maintained despite the sudden frequency change. Although it takes 7.5 ms to achieve frequency tracking, the new PD phasemeter can significantly increase frequency tracking performance. In space gravitational wave detection applications, it can increase the capture bandwidth and increase the anti-interference capability and stability. Moreover, the delay of 7.5 ms re-locking is far beyond the space gravitational wave detection frequency band of 0.1 mHz–1 Hz, which will not bring additional impact on space gravitational wave detection.

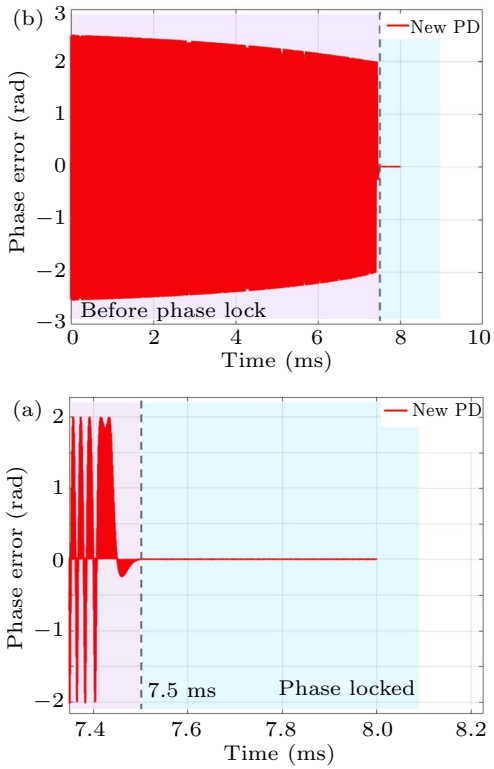


Fig. 6. The phase error of the phasemeter based on the new PD. (a) Time domain of phase error when the signal frequency changes abruptly from 10 MHz to 10.62 MHz. (b) Phase error of the new PD phasemeter when phase lock is achieved again after the signal frequency changes abruptly.

4.3. Experimental validation of new PD phasemeter

For experimental validation, an experimental framework of phasemeter frequency measurement dynamic range is established, as shown in Fig. 7(a). Different-frequency sine voltage signals are generated by a waveform generator (Keysight 33512B) and input to ADC for sampling as digital signals. The FPGA chip of the phasemeter is Altera EP4CE10 with a crystal oscillator frequency of 50 MHz. The frequency signals measured by the phasemeter are output to a PC running LabVIEW to record the data. Due to the limitation of ADC sampling frequency and FPGA chip performance, the dynamic range of frequency measurement of the phasemeter is verified by varying the frequency of the sine signal input to the phasemeter between 0.1 MHz and 4.9 MHz. As shown in Fig. 7(b), as the frequency of the sine input signal varies between 0.1 MHz and 4.9 MHz, the frequency signal of the phasemeter quickly realizes the frequency tracking within 0.4 s. Figure 7(c) shows the change in frequency readout of the new PD phasemeter during a sudden change in frequency, magnified locally from Fig. 7(b). It can be seen that after the sudden change in frequency, the phasemeter re-tracks the new frequency within 0.4 s. Through the above experimental verification, it is demonstrated that the phasemeter can track sudden frequency changes up to 4.8 MHz. Figure 7(d) demonstrates the frequency readout performance of the new PD phasemeter at different levels of frequency sudden change. The frequency tracking performance of the new PD phaseme-

ter is analyzed under different frequency mutation scenarios by switching among the input signal frequencies of 4.9 MHz, 3.8 MHz, 3.1 MHz, 2.8 MHz, 2.5 MHz, 2.2 MHz, 1.9 MHz, 1.3 MHz, and 0.1 MHz. It can be seen in Fig. 7(d) that the new PD phasemeter achieves fast and accurate frequency tracking during different frequency changes. The experimental validation of the new PD phasemeter's frequency tracking capability was conducted for signals up to 4.9 MHz. It is important to note that the current study serves as a proof-of-concept demonstration. The observed upper frequency limit is primarily defined by the hardware constraints of the present setup. Future work will involve implementing the proposed architecture with higher-speed electronics to validate and further enhance its performance, thereby fully meeting the demanding requirements of space-based gravitational wave detection.

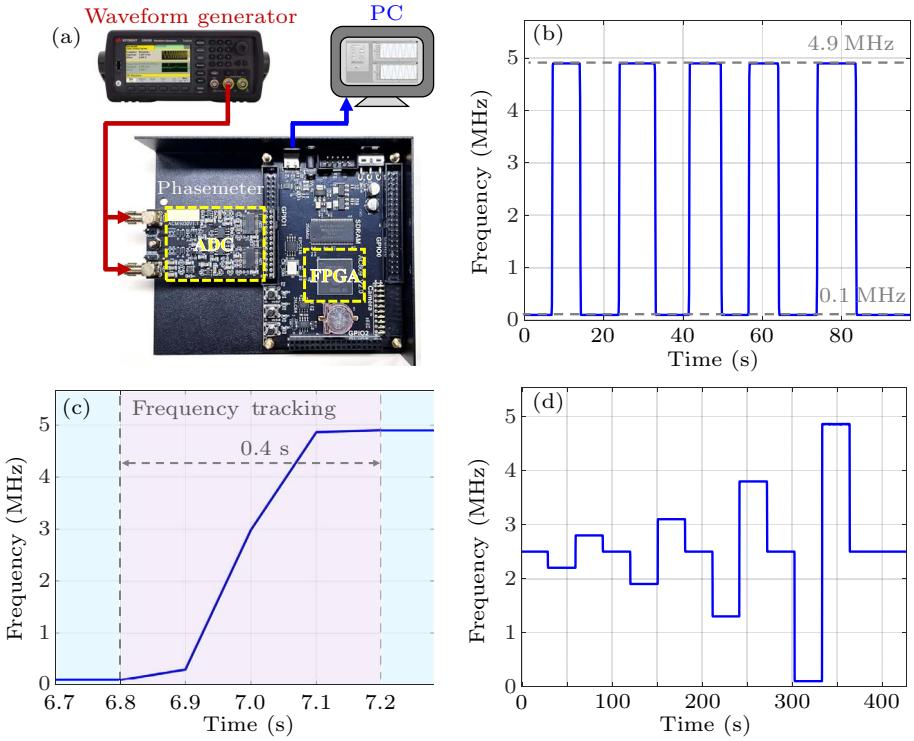


Fig. 7. Experimental verification of phasemeter frequency measurement dynamic range. (a) Experimental framework of phasemeter frequency measurement dynamic range. (b) New PD phasemeter frequency readout performance at a sudden frequency change of 4.8 MHz. (c) Frequency tracking time of the new PD phasemeter at the sudden frequency change of 4.8 MHz. (d) Frequency readout performance of the new PD phasemeter at different levels of sudden frequency change.

The phase readout noise of the new PD phasemeter was characterized by acquiring its output over an extended period. The linear spectral density of the resulting long-term phase data is presented in Fig. 8. To distinguish and subtract the low-frequency common-mode phase noise originating from laboratory environmental fluctuations (e.g., temperature drift), phase data from two independent channels were measured simultaneously. In Fig. 8, the red and blue curves represent the phase noise of the two individual channels, respectively. The purple curve depicts the phase noise level obtained by subtracting the time-domain data of the two channels, which effectively cancels the common-mode noise and reveals the intrinsic noise floor of the phasemeter itself. The results indicate that the measured phase noise of the current laboratory prototype does not fully meet the stringent requirement for space-based gravitational wave detection (e.g., < 5 μrad/Hz$^{1/2}$). This performance limitation, however, is attributed to the constraints of the current hardware platform, specifically the performance of the analog-to-digital converter (ADC), rather than representing a fundamental flaw in the novel second-harmonic filtering concept. The dominant noise sources in the present experimental setup are the quantization noise and sampling jitter introduced by the ADC. This hardware bottleneck currently masks the intrinsic potential of the new PD phasemeter architecture. The core contribution of this work lies in introducing and validating a new phasemeter architecture that solves the critical problem of dynamic range limitation caused by the second harmonic signal. The successful frequency tracking performance under large frequency steps, as demonstrated in Fig. 7, confirms this primary advantage. The phase noise measurements confirm that the proposed method functions as intended without introducing additional noise sources. The primary objective of this study was to establish the architectural feasibility. Future work will focus directly on implementing this design with a high-performance ADC and a low-jitter clock source, which constitutes a straightforward path toward

achieving the target phase noise level for space gravitational wave detection missions.

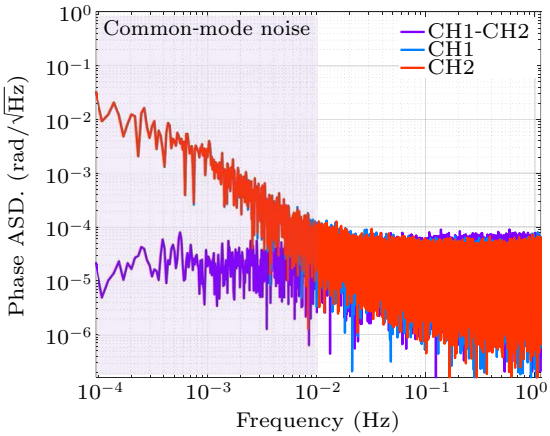


Fig. 8. Amplitude spectral density of phase measurement noise for the new PD phasemeter.

5. Conclusion and perspectives

Due to the relative motion between satellites and the scientific requirements of SGWD, phasemeters must achieve high phase readout accuracy, a greater dynamic range, and resistance to sideband signal interference. In phasemeters that typically use the phase-locked loop principle, the second harmonic signal generated by the mixer limits both the dynamic range and phase measurement accuracy. By briefly outlining the basic principles of the interstellar laser interferometer and the normal PD phasemeter, this paper analyzes two effects of the second harmonic signal produced by the mixer on phasemeter performance. Normal PD phasemeters incorporate a low-pass filter in the loop, which introduces phase delay and limits both the dynamic range and response speed of the phasemeter. Building on this analysis of the second harmonic signal's impact, a new phasemeter based on a second harmonic signal filter is proposed. Unlike the normal PD phasemeter, the cut-off frequency of the second harmonic signal filter in the new PD phasemeter varies with the frequency of the mixer output signal. This real-time subtraction of the second harmonic signal effectively eliminates it, reducing loop phase delay. Furthermore, an analysis of the noise sources in the new PD phasemeter reveals that the primary noise source is sampling time jitter, which can be effectively suppressed through pilot-tone correction, achieving a noise level better than 5 μrad/Hz$^{1/2}$. Finally, digital fixed-point simulations are employed to verify the functionality of the new PD phasemeter. Compared to the normal PD phasemeter, the new PD phasemeter achieves frequency tracking and phase locking within just 7.5 ms following a sudden change in the input signal frequency. Finally, it is experimentally verified that the phasemeter can can track a sudden frequency change of up to 4.8 MHz. The quantitative evaluation of second-harmonic signal suppression is difficult to ascertain directly from the phasemeter's own readouts. To address this, a future study will develop a dedicated test platform utilizing a signal analyzer to quantitatively benchmark the suppression performance. Looking ahead, our research will proceed in two key directions: firstly, the ground-based validation of the phasemeter within a representative laser interferometry system, and secondly, the engineering development of a flight-like prototype. In space-based gravitational-wave detection, the new PD phasemeter ensures stable frequency tracking and phase readout during abrupt frequency changes, thereby enhancing operational stability during gravitational-wave detection. Furthermore, this high-precision phasemeter, capable of operating across a broad frequency range, can also be applied in fields such as laser communication and laser ranging.

Acknowledgements

The authors thank the National Key Research & Development Program of China (Grant No. 2022YFC2203901), the State Key Laboratory of Spatial Datum (Grant No. SKLSD2025-KF-03), Fundamental Research Funds for the Central Universities, and Sun Yat-sen University for the support.

References

[1] Gong Y, Luo J and Wang B 2021 *Nat. Astron.* **5** 881
[2] Cai R G, Cao Z, Guo Z K, Wang S J and Yang T 2017 *Natl. Sci. Rev.* **4** 687
[3] Huang S J, Hu Y M, Korol V, Li P C, Liang Z C, Lu Y, Wang H T, Yu S and Mei J 2020 *Phys. Rev. D* **102** 063021
[4] Liu S, Hu Y M, Zhang J and Mei J 2020 *Phys. Rev. D* **101** 103027
[5] Feng W F, Wang H T, Hu X C, Hu Y M and Wang Y 2019 *Phys. Rev. D* **99** 123002
[6] Bao J, Shi C, Wang H, Zhang J, Hu Y, Mei J and Luo J 2019 *Phys. Rev. D* **100** 084024
[7] Wang H T, Jiang Z, Sesana A, Enrico Barausse, Huang S J, Wang Y, Feng W F, Wang Y, Hu Y, Mei J and Luo J 2019 *Phys. Rev. D* **100** 043003
[8] Danzmann K and team the L study 1996 *Class. Quantum Grav.* **13** A247
[9] Luo J, Chen L S, Duan H Z, Gong Y G, Hu S, Ji J, Liu Q, Mei J, Milyukov V, Sazhin M, Shao C G, Toth V T, Tu H B, Wang Y, Wang Y, Yeh H C, Zhan M S, Zhang Y, Zharov V and Zhou Z B 2016 *Class. Quantum Grav.* **33** 035010
[10] Kawamura S, Hiroo Kunimori, Hosokawa M, Fujita R, Maeda K, H. Shinkai, Tanaka T, Wakabayashi Y, Ishihara H, Nishiyama K, Ueda K, Kaiki Taro Inoue, Yamamoto K, Kunihito Ioka, Hong F, Y. Tsunesada, Numata K, Shibata M, Hitoshi Kuninaka and Hayama K 2011 *Class. Quantum Grav.* **28** 094011
[11] Hu W R and Wu Y L 2017 *Natl. Sci. Rev.* **4** 685
[12] Ming M, Luo Y, Liang Y R, Zhang J Y, Duan H Z, Yan H, Jiang Y Z, Lu L F, Xiao Q, Zhou Z and Yeh H C 2020 *Int. J. Extrem. Manuf.* **2** 022003
[13] Mei J, Bai Y Z, Bao J, Barausse E, Cai L, Canuto E, Cao B, Chen W M, Chen Y, Ding Y W, Duan H Z, Fan H, Feng W F, Fu H, Gao Q, Gao T, Gong Y, Gou X, Gu C Z and Gu D F 2020 *Prog. Theor. Exper. Physics* **5** 059201
[14] Wand V, GuzmaánF, Heinzel G and Karsten Danzmann 2006 *AIP Conf. Proc.* **873** 689
[15] Bykov I, José J, Francisco A, Heinzel G and Karsten Danzmann 2009 *J. Phys.: Conf. Ser.* **154** 012017

[16] Gerberding O, Sheard B, Bykov I, Kullmann J, José J K 2013 *Class. Quantum Grav.* **30** 235029
[17] Liang Y R, Duan H Z, Xiao X L, Wei B B and Yeh H C 2015 *Rev. Sci. Instrum.* **86** 016106
[18] Liang Y R 2018 *Rev. Sci. Instrum.* **89** 036106
[19] Jiang Y Z, Jin X L, Yeh H C and Liang Y R 2021 *Opt. Express* **29** 18336
[20] Yang R, Liu H and Luo Z 2024 *IEEE Trans. Instrum. Meas.* **73** 7006508
[21] Huang X, Wang G, Yang M, Yang Z, Cai C, Ming M, Zhang J, Yang S, Tu L, Duan H, Li Z and Yeh H 2023 *Opt. Laser Technol.* **161** 109185
[22] Zheng L, Yang S and Zhang X 2023 *Phys. Rev. D* **108** 022001
[23] Zhou M Y, Hu X C, Ye B, Hu S, Zhu D D, Zhang X, Su W and Wang Y 2021 *Phys. Rev. D* **103** 103026
[24] Liang Y R, Duan H Z, Yeh H C and Luo J 2012 *Rev. Sci. Instrum.* **83** 095110
[25] Liang Y R, Feng Y J, Xiao G Y, Jiang Y Z, Li L and Jin X L 2021 *Rev. Sci. Instrum.* **92** 124501
[26] Wang D, Zhang X and Duan H 2024 *Class. Quantum Grav.* **41** 117003
[27] Fang Y, Zhang X, Fu F and Li H 2024 *Phys. Rev. D* **109** 062001
[28] Wei C Q, Liu J B, Dong Y F, Sun Y N, Zhou Y, Zheng H B, Liu Y Y, Yan X S, Li F L and Xu Z 2024 *Chin. Phys. B* **33** 034203
[29] Wu J, Li J and Jiang Q 2023 *Chin. Phys. B* **32** 090401
[30] Zhang J D and Wang S 2022 *Chin. Phys. B* **32** 010306
[31] Zhang Z G, Dong F L, Cheng T, Qian K M, Qiu K, Zhang Q C, Chu W G and Wu X P 2014 *Chin. Phys. Lett.* **31** 114208
[32] Feng Y J, Jiang Y Z, Xiao G Y, Chen L Y, Lu B F, Xu Z L and Liang Y R 2024 *Rev. Sci. Instrum.* **95** 104503